Solution-Processed Transparent Self-Powered p-CuS-ZnS/n-ZnO UV Photodiode

Xiaojie Xu, Sudhanshu Shukla, Ya Liu, Binbin Yue, James Bullock, Longxing Su, Yanmei Li, Ali Javey, Xiaosheng Fang,* and Joel W. Ager*

Transparent diodes formed by a heterojunction between p-type CuS–ZnS and n-type ZnO thin films were fabricated by sequential chemical bath deposition and sol-gel spin coating. The diodes are transparent in the visible ($\approx$70% at 550 nm) and exhibit a good rectifying characteristics, with I_f/I_r ratios of up to 800 at $\pm$1 V, higher than most of the reported solution-processed diodes measured at a similar bias. More importantly, when operated as a self-powered (zero bias) UV photodetector, they show stable and fast (<1 s) photoresponse with a maximum responsivity of 12 mA W^{-1} at 300 nm. Both the response time and responsivity of the p-CuZnS/n-ZnO UV photodiode are comparable or superior to similar solution-processed devices reported in the literature.

In the last decades, "transparent electronics" and "invisible circuits" have drawn increasing interest in the context of next-generation optoelectronic and consumer devices.[1–4] Transparent conducting materials (TCMs) which possess good optical transparency and electrical conductivity are essential components of these devices.[5–7] As a p–n junction is the key building block of most semiconductor devices, both transparent hole- and electron-conducting materials will be required to achieve full

functionality.[8] However, most of the well-known TCMs are n-type,[9–11] such as ZnO,[12,13] Al-doped ZnO (AZO),[14–17] and Sn-doped In$_2$O$_3$ (ITO).[6,18] In contrast, p-type TCMs are less well developed.[19–21] Therefore, it is of interest to explore p-type TCMs which can not only be fabricated by facile and cost-effective methods, but also be process compatible with widely used n-type TCMs.[22] Although vacuum-based deposition methods are widely explored to form a high quality p–n junction of these materials, recent developments on solution-based deposition techniques have made it plausible to deposit such multicomponent materials with a simple and cost effective method.

There is also a recent emphasis on lowering the power consumption of devices.[23,24] Among various applications, development of photodetectors has received significant attention. Combination of appropriate band gap materials can be utilized for ultrafast detection of photons in particular part of electromagnetic radiation. The fast response time to the light and high sensitivity to the wavelength is desirable. Also it is advantageous to make them operate without external bias in self-powered mode.[25] In particular, self-powered UV photodetectors are of interest for prospective applications in chemical and biological analysis and in communications.[26] Detection of UV light (200–400 nm) is of special interest as part of the UV light will not be absorbed by the stratospheric ozone layer and its overexposure has been linked to the development of skin cancers. UV photodetectors usually contain a Schottky or a p–n heterojunction and separate the photogenerated electron–hole pairs through the photovoltaic effect.[27–31] Many of the reported self-powered UV detectors required vacuum processing and/or high temperature for their synthesis, which will limit scalability.[26,32] It is thus of interest to develop a process for making UV photodetectors using scalable, low-temperature processing.

In this work, we present a transparent p-CuS-ZnS/n-ZnO heterojunction diode constructed by low-temperature solution phase processing. ZnO with a band gap of 3.37 eV was chosen as it is a component of some of the better performing UV detectors.[33–36] In general, the rectifying behavior of solution-processed transparent diodes is inferior compared to those made with vacuum-based techniques.[37] But recent advancements in the solution-processed devices are encouraging. Park et al.[38] reported a NiO/ZnO photodiode prepared by sol-gel processing and observed a rectification ratio (I_f/I_r) of 50 at $\pm$5 V. Deo et al.[39]

Dr. X. J. Xu, Dr. L. X. Su, Y. M. Li, Prof. X. S. Fang
Department of Materials Science
Fudan University
Shanghai 200433, P. R. China
E-mail: xshfang@fudan.edu.cn

Dr. X. J. Xu, Dr. S. Shukla, Dr. Y. Liu, Prof. A. Javey, Prof. J. W. Ager
Materials Sciences Division
Lawrence Berkeley National Laboratory
Berkeley, CA 94720, USA
E-mail: jwager@lbl.gov

Prof. J. W. Ager
Materials Science and Engineering
University of California at Berkeley
Berkeley, CA 94720, USA

Dr. J. Bullock, Prof. A. Javey
Electrical Engineering and Computer Sciences
University of California
Berkeley, CA 94720, USA

Dr. B. B. Yue
Advanced Light Source
Lawrence Berkeley National Laboratory
Berkeley, CA 94720, USA
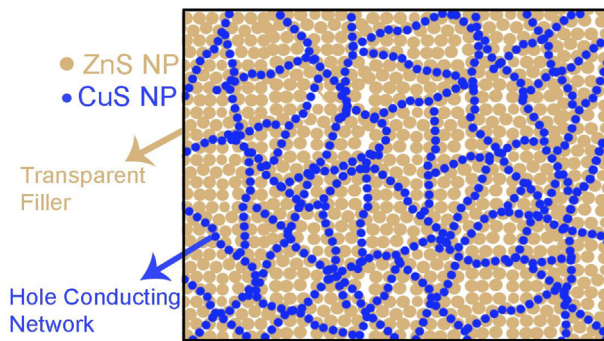
Scheme 1. Illustration of the hole conducting mechanism of p-type transparent CuS–ZnS nanocomposite film.

reported a Cu$_2$O/ZnO heterojunction diode fabricated by hydrothermal synthesis with an I_f/I_r ratio of 200 at ±3 V. Ichimura and Maeda[40] reported a diode constructed by photochemically deposited Cu$_x$Zn$_y$S and electrochemically deposited ZnO with a moderate rectifying behavior.

There also has been prior work on low temperature processing of ZnO-based self-powered UV detectors. For example, Tian et al.[36] prepared a ZnO/SnO$_2$ heterojunction nanofiber UV photodetector via electro-spinning. While the device had a high transmittance of ≈90% in visible range and good responsivity at the bias of 10 V, the rise time (T_r) and decay time (T_d) for UV response were relatively slow, 32.2 and 7.8 s, respectively. Teng et al.[41] reported a ZnO/Cu nanowire UV detector with a self-powered UV responsivity of 0.65 mA W^{-1}, response speed of 0.5 s (T_r) and 30 s (T_d), and an average transparency of 40%. In contrast, many other ZnO-based UV detectors have either slow response or low responsivity under zero bias,[41–45] or are not highly transparent in the visible.[41,44]

In our previous work, we have demonstrated excellent transparency and high hole conductivity in (CuS)$_x$–(ZnS)$_{1-x}$

nanocomposite films, where CuS and ZnS nanocrystals (less than 10 nm) are homogenously distributed within the films, as illustrated in **Scheme 1**. The p-type conductivity is believed to come from the hole conducting network formed by CuS nanocrystals (p-type) and it increases with the content of CuS, while the ZnS nano-domains serve as the transparent fillers. Thus, it enables the nanocomposite film to possess both transparency and hole conductivity.[46–48] Here, (CuS)$_{0.35}$:(ZnS)$_{0.65}$ is chosen as the candidate to realize a p–n junction with n-ZnO. (CuZnS will be written in short for (CuS)$_{0.35}$:(ZnS)$_{0.65}$ through the text.) The heterojunction p-CuZnS/n-ZnO devices in this work have a high rectifying behavior ($I_f/I_r = 800$ at ±1 V), which is superior to many previously reported solution-processed transparent diodes.[37] When operated as a self-powered UV photodetector, it has a fast response speed and a maximum responsivity at zero bias of 12 mA W^{-1} at 300 nm, which makes it an outstanding transparent self-powered UV detector.

The transparent diode structure (glass/FTO/CuZnS/ZnO/Al) used in this work is depicted in **Figure 1**(a). With the exception of the Al contact, which was deposited by e-beam evaporation, all other layers of the devices were prepared by low-temperature solution processes. FTO-glass substrates (1 inch square) were first coated with a nanocomposite film of p-type CuS-ZnS via two steps of chemical bath deposition (CBD), followed by four layers of n-type ZnO deposited with sol-gel spin coating. After each coating of ZnO, the device was annealed at 300 °C for 2 min on a hot plate to evaporate the organic solvent from the ZnO sol-gel. The thickness of the p- and n-TCM were optimized to eliminate pinholes in each layer with 2 cycles of CBD and 4 cycles of spin coating producing the best results. Complete details of CuS–ZnS and ZnO deposition are provided in the Experimental Section.

Figure 1(b) is a cross-section scanning electron microscopy (SEM) image of the device structure. The thicknesses of n-ZnO and p-CuZnS layers are about 200 and 70 nm, respectively. Even though the surface smoothness of the FTO/ glass substrate is not
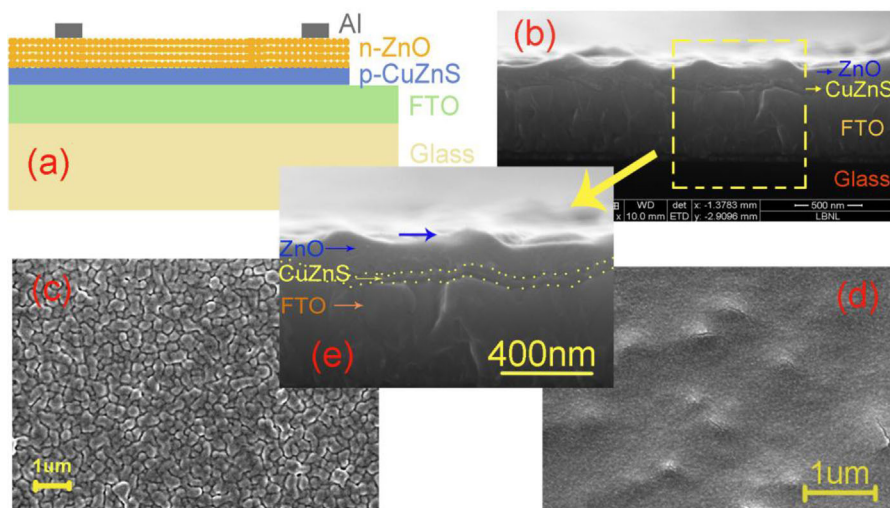
Figure 1. (a) Schematic illustration of the device structure; (b) cross-section SEM image of the layers in device; (c) and (d) top view SEM images of ZnO and CuZnS layers, respectively; (e) the magnified cross-section SEM image of the area marked in yellow dash line from (b).
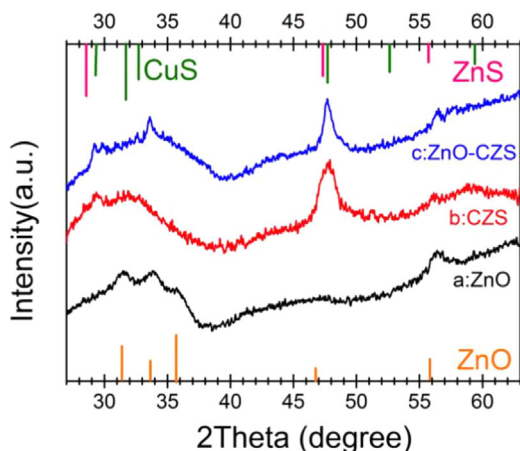
Figure 2. XRD patterns of n-ZnO and p-CuZnS films and of the CuZnS/ZnO heterojunction. 2θ values are for the Cu Kα scale and were converted from the Q values determined by the synchrotron measurement (see Experimental Section for details).

ideal, the chemical-bath-deposited CuZnS thin film still forms a compact and continuous layer on top of the substrate. With a closer observation at the interface of the p–n junction, as shown in Figure 1(e), the ZnO and CuZnS layer form a well-interacted interface after the annealing process of ZnO deposition. To study the morphology of the solution-processed n and p layer, ZnO and CuZnS layers were grown separately on glass substrates for plan view SEM image characterization, as can be seen in Figure 1(c) and (d), respectively. Both films are composed of uniform, dense-packed nanoparticles without noticeable pinholes in large scale. However, the mean grain size of ZnO film is apparently larger than that of CuZnS film. For the CuZnS, we have previously shown that we can achieve the ion by ion growth regime required to form a nanocomposite with small domains.[47] In contrast, the ZnO film was obtained by the coating of pre-nucleated and grown ZnO nanoparticles, which results in relatively larger grains.

Synchrotron X-ray diffraction was used to identify the crystalline phases present in the separately grown ZnO and CuZnS films and in the CuZnS/ZnO heterojunction structure. As shown in **Figure 2**, all the peaks from the ZnO film can be indexed to hexagonal ZnO, while the broad peaks from the CuZnS film indicate two sets of crystal phases, cubic ZnS and covellite CuS, which is consistent with our previous work.[47] Also the broader peaks from CuS–ZnS film again suggests the smaller crystal domain size compared to that of ZnO. For the p–n junction structure, signals from both ZnO and CuS–ZnS are present and the relatively sharper peaks suggest a quantitatively better crystallinity of the CuS–ZnS layer after the fast annealing process for coating of ZnO layer. In comparing the XRD patterns of each layer before and after the formation of the ZnO/CuS–ZnS heterojunction, no new phases are observed; however, we cannot completely rule out the possibility of new phase formed at the interface.

Figure 3 shows transmission and reflectance spectra of the solution processed ZnO and CuS–ZnS films and of the diode device. The CuZnS film has a transmittance of ≈65% at 550 nm, while ZnO layer clearly has a higher transparency of >90% over the wavelength of 400–850 nm. The sharp absorption edge at ≈375 nm of ZnO film corresponds to the band gap of ZnO (3.3 eV). And the estimated direct optical band gap of the nanocomposite $(CuS)_{0.35}$-$(ZnS)_{0.65}$ is around 3.4 eV (see details in Figure S2, Supporting Information). As a p-type CuS–ZnS film is composed of the mixed phases of ZnS and CuS, it has the absorption features of both ZnS and CuS, resulting in a relatively broad absorption edge extending from 350–500 nm. It is interesting to note that the transmittance of the p–n junction, an average of nearly 70% in the visible range, is higher than that of CuS–ZnS layer by itself. As indicated by the corresponding reflectance spectra in Figure 3b, the ZnO layer on top of CuS–ZnS film serves as anti-reflection coating layer as the reflection of CuS–ZnS is decreased after the deposition of ZnO. Compared with the smooth surface of CuS–ZnS film, the ZnO film composed of larger grains is relatively rougher, which give rises to the decrease of the reflectance of CuZnS/ZnO heterojunction. The enhancement of transparency in visible range will be beneficial for the performance of TCM-based optoelectronic devices.

Current–voltage (I–V) characteristics of the p-CuZnS/n-ZnO heterojunction device and two control samples measured in the
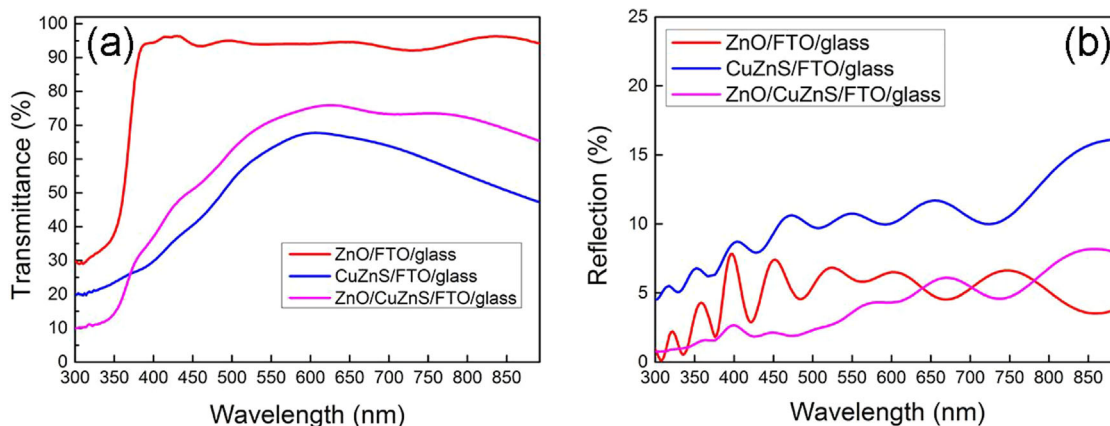
Figure 3. (a) Transmittance and (b) reflectance spectra of n-ZnO, p-CuZnS, and the CuZnS/ZnO heterojunction on FTO/glass substrates.

ADVANCED SCIENCE NEWS
www.advancedsciencenews.com

pss rrl
physica status solidi
www.pss-rapid.com

dark are shown in **Figure 4**. A linear current–voltage curve is observed for control structures of ITO/ZnO/Al and ITO/CuZnS/Al, while the device consisting of CuZnS/ZnO reveals non-linear rectifying behavior, indicating the successful formation of p–n junction. The turn-on voltage is found to be around 1 V, similar to the transparent ZnO/NiO diode reported by Ohta et al.[45] The p-n diode exhibits a high rectification ratio of 800 at ± 1 V bias.
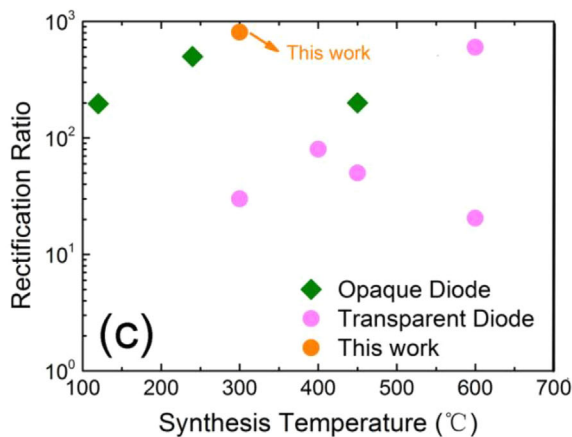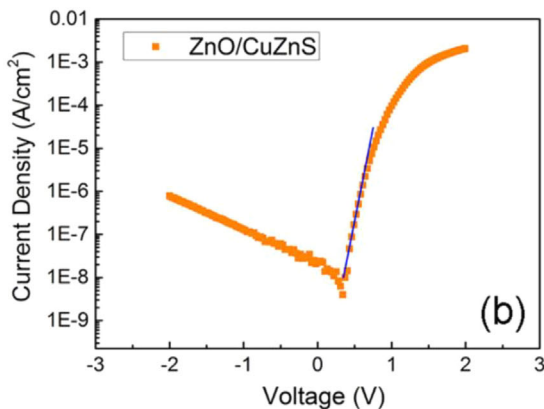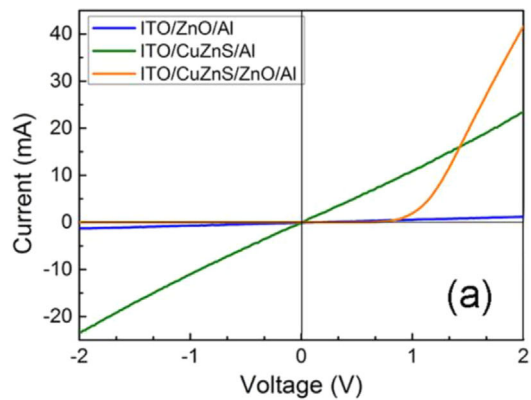
Figure 4. Linear (a) and semilog (b) plots of current density versus voltage for the CuZnS/ZnO diode; (c) rectification ratio of forward and reverse current at $\pm V_0$ versus the synthesis temperature for transparent solution-processed diodes. See Table 1 for sources of the literature reports and for the values of V_0.

Extra attention should be paid to the fast annealing process when fabricating ZnO film, as a longer and/or high-temperature annealing process may cause Cu diffusion from CuZnS layer into ZnO layer, resulting in a possible shunt path at the interface that deteriorates the device performance. As shown in Figure 4(b), the ideality factor n obtained from the dark J–V plot is calculated to be ≈ 2.1 (see detailed fitting method in Figure S1 and S2, Supporting Information). The non-ideal ideality factor (>2) suggests an additional process plays an important role in conduction. This behavior has been reported in similar devices and attributed to tunneling current at the p–n junction.[49–51] To fully understand the origin of the non-ideal ideality factor, further investigation will be needed. This diode shows a small current at 0 bias, which has been seen in other diodes with high rectification ratios and has been attributed to capacitive charging[52]; Figure S3, Supporting Information shows a forward and reverse voltage sweep; a hysteresis effect is observed. The effect may come from the capacitive charging and lead to a finite current at zero bias of the device during voltage sweeps.

Previously, Diamond et al.[53] reported a CuZnS/ZnO diode prepared by pulsed laser deposition at 550 °C and observed an on–off ratio of 75 at ± 3 V. Our diode, which was prepared by a simple, low-temperature, low-cost solution method, shows a superior rectifying behavior. To further compare the rectifying characteristics of this device with other solution-processed diodes, **Table 1** lists the performance and fabrication methods of a number of diodes using various p layers such as NiO, Cu_2O, and $CuAlO_2$. Figure 4c maps out the rectification ratio of the solution-processed diodes from Table 1 versus their synthesis temperature. The p-CuZnS/n-ZnO diode compares favorably with other solution-processed diodes by having a relatively higher on/off ratio combined with optical transparency and a low synthesis temperature. The high rectification ratio of our diode may be ascribed to quality of the interface between n-ZnO and p-type CuZnS. The four cycles of ZnO deposition are believed to reduce the density of pin-holes in the n-type layer. Each fast annealing process (2 min) after coating of the ZnO on top of CuZnS might also improve contact at the interface.

Table 1. Comparison of parameters of solution-processed diodes.

Device structure	Method	Max I_f/I_r	$\pm V_0$	T (°C)	Ref.
NiO/ZnO	SG/SG	50	5	450	[38]
NiO/MgZnO	SG/SG	20.5	3.5	600	[55]
NiO/TiO$_2$	SG	80	4	400	[56]
Li:NiO/ITO	SP	600	2	600	[57]
Cu$_2$O/ZnO	HT	200	3	450	[39]
MoO$_3$/FeS$_2$/ZnO	RFS/SC	500	1	240	[58]
CuI/FeS$_2$/ZnO	HT/SC	197	1	120	[59]
CuAlO$_2$/AZO	SG	30	4	300	[60]
CuZnS/ZnO	CBD/SG	800	1	300	This work

SC, spin coating; SG, sol-gel; SP, spray pyrolysis; ECD, electrochemical deposition; RFS, RF sputtering; HT, hydrothermal synthesis; CBD, chemical bath deposition. The temperature listed above refers to the highest temperature required in the fabrication process.

Typically, response speed and responsivity are two key parameters for a photodetector and are usually used to evaluate the figure of merit in a photodetector. **Figure 5**a shows the photoresponse of p-CuZnS/n-ZnO diode at zero bias and Figure 5b displays the enlarged portion of the range of 19–27 s showing that the T_r and T_s of this device are 0.7 and 0.86 s, respectively. Notably, both are less than 1 s, which is faster than that of many other solution-processed self-powered photodetectors listed in **Table 2**. During five switching cycles, the device exhibits a stable reproducible photoresponse, which is further confirmed by more cycles of on–off testing shown in Figure S5, Supporting Information. The photocurrent under illumination at 0 V bias indicates a small open circuit voltage generated from the p–n junction.

The external quantum efficiency (EQE) under zero bias voltage of p-CuZnS/n-ZnO diode is shown in Figure 5c. The EQE spectra at UV range (300–370 nm) matches well with the absorption spectra of ZnO (3.3 eV) and CuZnS (3.4 eV) shown in Figure S4, Supporting Information. The EQE value becomes negligible at wavelength longer than 370 nm, which agrees well with the absorption spectra, and shows that the UV detector is insensitive to visible light. As seen in Figure 5d, the maximum responsivity at zero bias of the as-prepared transparent UV photodetector is 12 mA W^{-1} at 300 nm, which is superior to many other solution-processed self-powered UV detectors, as

listed in Table 2. To the best of our knowledge, among the few solution-processed transparent UV detectors in literature, our p-CuZnS/n-ZnO UV photodiode shows a unique combination of fast photoresponse and excellent responsivity.

In summary, we demonstrated a transparent self-powered UV photodiode based on the structure of p-CuS-ZnS/n-ZnO. The heterojunction was fully prepared by cost-effective, scalable solution processes. The device exhibits an excellent rectifying behavior with I_f/I_r ratio of 800 at ±1 V, higher than most of the reported solution-processed diodes at similar bias. It shows fast and stable photoresponse and excellent responsivity (12 mA W^{-1}) to UV light under zero bias, making it a promising self-powered transparent UV photodetector. The promising optoelectronic properties of non-toxic, earth-abundant, low-cost solution processable p-type transparent conductive CuS–ZnS thin film offers potential for the development of scalable and low cost transparent electronics.

Experimental Section

Preparation of p-Type CuS-ZnS: Three solutions were prepared: (a) 0.06 g CuSO$_4$ and 1.68 g Zn(CH$_3$COO)$_2$ together in 100 ml of DIW; (b) 0.96 g Na$_2$EDTA in 50 ml of DIW; and (c) 0.6 g C$_2$H$_5$NS in 50 ml of DIW. First, solution (b) was added into
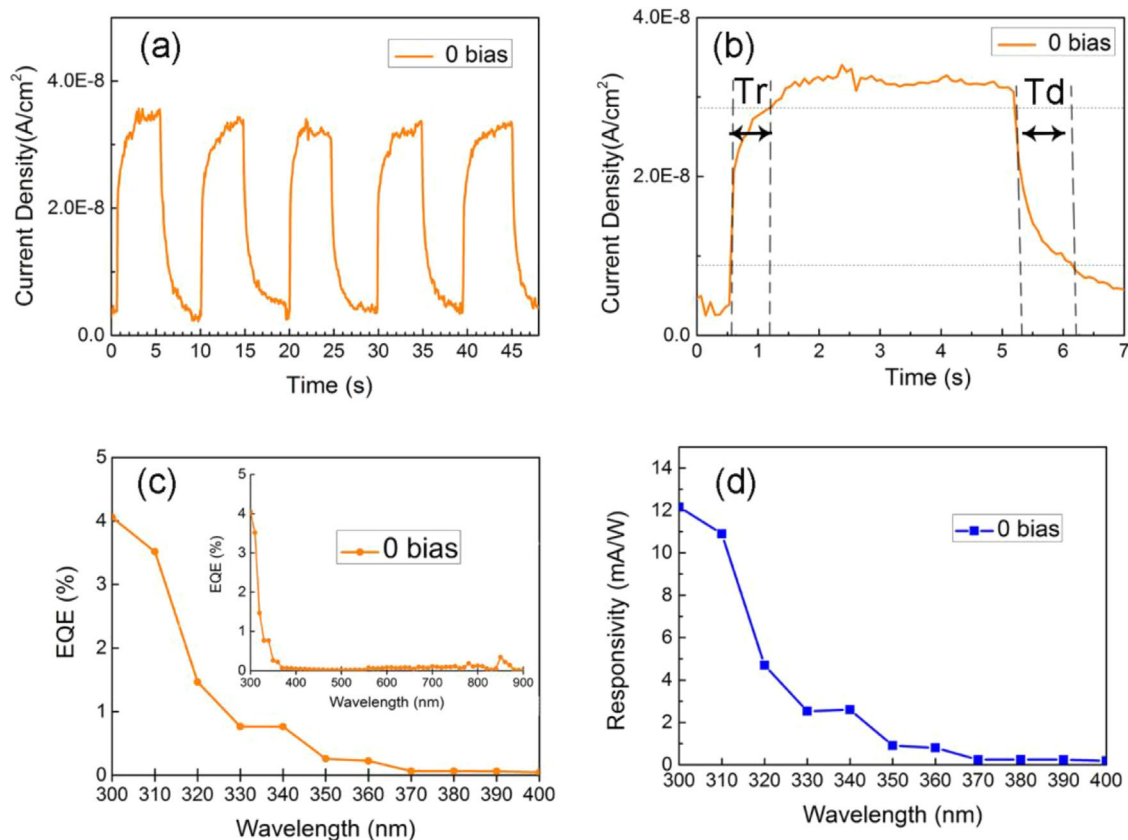
Figure 5. (a) Time dependence of the current density of a CuZnS/ZnO photodiode measured at 0 bias under AM1.5 illumination; (b) the corresponding T_r and T_d of CuZnS/ZnO photodetector, T_r: 10–90% maximum photocurrent, T_d: 90–10% maximum photocurrent; (c) EQE of CuZnS/ZnO photodiode versus wavelength; (d) the corresponding wavelength-dependent responsivity spectrum.

Table 2. Comparison of the characteristic parameters of self-powered UV photodetectors.

Year	Journal	Structure	Bias	λ (nm)	R (mA W^{-1})	Tr/Td (s)	T (%)
2016[29]	ACS ASI	TiO_2–PANI	0	350	3.6	<1/<1	Opaque
2013[36]	AM	ZnO–SnO_2	10	300	–	32.2/7.8	90%
2016[41]	JMCC	Cu NW/ZnO	0	360	0.65	0.5/30	40%
2013[61]	APL	TiO_2/MeOTAD	0	410	10	0.12/0.06	70%
2016[42]	Nanotechnology	Graphene/ZnO	0	365	0.55	3/0.5	–
2012[43]	JMCC	rGO/ZnO	0	334	–	<1/20	Opaque
2016[62]	JMCC	TiO_2/NiO	0	350	0.06	1.2/7.1	Opaque
2016[44]	Small	MgZnO–PANI	0	260	0.16	0.3/0.3	Opaque
2017	This work	CuZnS/ZnO	0	300	12	0.7/0.86	80%

λ, wavelength (nm); R, responsivity (mA W^{-1}); Tr/Td, rise time and decay time (s); T, transmittance at 550 nm (%).

(a) and mixed in ultrasonic bath for 10 min. Then solution (c), the sulfur precursor, was added to the mixture and immediately the pretreated substrate was immersed vertically in the solution. The beaker was sealed and placed on a hot plate system under the condition of constant stirring at 80 C. After 1 h, the substrate was removed from the reaction solution, washed with DIW and dried by an N_2 gun.

Preparation of n-Type ZnO: To make ZnO films via sol–gel spin coating, we adapted the procedure of Panthani et al.[54] One gram zinc acetate was mixed with 10 ml 2-methoxyethanol and 0.3 ml ethanolamine. The mixture was stirred for 1 h then ultrasonicated for 1 h. Then the solution was then filtered through a 0.2 µm filter, dropped on the CuS-ZnS film, and spin coated at 3000 rpm for 1 min. The substrate was placed on a hot place heated to 300 °C for 2 min, and then left at room temperature to cool.

Preparation of Contacts: Al contacts were fabricated by e-beam evaporation. A shadow mask was used to define the contact area.

X-Ray Characterization: The X-ray diffraction experiments were carried out at beamline 12.3.2 of the Advanced Light Source at Lawrence Berkeley National Laboratory. A monochromatic X-ray beam of 10 keV was focused on the thin film sample placed in reflection mode into the beam. A Pilatus 1M area detector was placed at 350-mm to record Debye rings diffracted by the sample. The exposure time for each sample was 180 s. An alumina standard was used to determine the beam center and sample to detector distance. The measurements were done at room temperature.

EQE analysis was performed by a home built set-up which was calibrated by a standard Si diode prior to diode testing. The photoresponsivity of a PD can also be estimated by the following equation:

$$EQE = (R_\lambda/\lambda) \times 1240 (\text{nm W A}^{-1}) \times 100\%,$$

where R_λ is the photo responsivity in A W^{-1} at a given wavelength of incident light and λ is the wavelength in nm. The *I–V* characteristics of the diodes was measured by Keithley 2400. The light *J–V* characteristics of these diodes was measured under standard conditions (AM 1.5G spectrum, 100 mW cm^{-2}, 25 °C).

Supporting Information

Additional electrical and optical characterization: forward/reverse voltage sweep, ideality factor calculation, absorption spectra and Tauc plot, current under on/off light switching cycles.

Conflict of Interest

The authors declare no conflict of interest.

[1] G. Thomas, *Nature* **1997**, *389*, 907.
[2] J. F. Wager, *Science* **2003**, *300*, 1245.

[3] A. Facchetti, T. J. Marks, *Transparent Electronics*. John Wiley & Sons, Ltd., Chichester, UK **2010**.

[4] E. Fortunato, P. Barquinha, R. Martins, *Adv. Mater.* **2012**, *24*, 2945.

[5] B. Szyszka, P. Loebmann, A. Georg, C. May, C. Elsaesser, *Thin Solid Films* **2010**, *518*, 3109.

[6] K. Ellmer, *Nat. Photon.* **2012**, *6*, 809.

[7] M. Morales-Masis, S. De Wolf, R. Woods-Robinson, J. W. Ager, C. Ballif, *Adv. Electron. Mater.* **2017**, *3*, 1600529.

[8] H. Hosono, *Thin Solid Films* **2007**, *515*, 6000.

[9] D. S. Ginley, C. Bright, *MRS Bull.* **2000**, *25*, 15.

[10] R. G. Gordon, *MRS Proc.* **1996**, *426*, 419.

[11] D. Ginley, H. Hosono, D. C. Paine, *Handbook of Transparent Conductors*. Springer US, Boston, MA **2010**.

[12] J.-H. Lim, C.-K. Kang, K.-K. Kim, I.-K. Park, D.-K. Hwang, S.-J. Park, *Adv. Mater.* **2006**, *18*, 2720.

[13] A. Klein, C. Körber, A. Wachau, F. Säuberlich, Y. Gassenbauer, S. P. Harvey, D. E. Proffit, T. O. Mason, C. Korber, A. Wachau, F. Sauberlich, Y. Gassenbauer, S. P. Harvey, D. E. Proffit, T. O. Mason, *Materials (Basel)* **2010**, *3*, 4892.

[14] B.-Y. Oh, M.-C. Jeong, T.-H. Moon, W. Lee, J.-M. Myoung, J.-Y. Hwang, D.-S. Seo, *J. Appl. Phys.* **2006**, *99*, 124505.

[15] M. L. Grilli, A. Sytchkova, S. Boycheva, A. Piegari, *Phys. Status Solidi A* **2013**, *210*, 748.

[16] H. Hagendorfer, K. Lienau, S. Nishiwaki, C. M. Fella, L. Kranz, A. R. Uhl, D. Jaeger, L. Luo, C. Gretener, S. Buecheler, Y. E. Romanyuk, A. N. Tiwari, *Adv. Mater.* **2014**, *26*, 632.

[17] A. Bikowski, M. Rengachari, M. Nie, N. Wanderka, P. Stender, G. Schmitz, K. Ellmer, *APL Mater.* **2015**, *3*, 60701.

[18] T. Minami, *Thin Solid Films* **2008**, *516*, 5822.

[19] A. N. Banerjee, K. K. Chattopadhyay, *Prog. Cryst. Growth Charact. Mater.* **2005**, *50*, 52.

[20] G. Hautier, A. Miglio, G. Ceder, G.-M. Rignanese, X. Gonze, *Nat. Commun.* **2013**, *4*, 2292.

[21] K. H. L. Zhang, K. Xi, M. G. Blamire, R. G. Egdell, *J. Phys.: Condens. Matter* **2016**, *28*, 383002.

[22] C. Yang, M. Kneiß, F.-L. Schein, M. Lorenz, M. Grundmann, *Sci. Rep.* **2016**, *6*, 21937.

[23] C. Piguet, Ed., *Low-Power Electronics Design*. CRC Press, Boca Raton **2004**.

[24] D. J. Gundlach, *Nat. Mater.* **2007**, *6*, 173.

[25] L. Peng, L. Hu, X. Fang, *Adv. Funct. Mater.* **2014**, *24*, 2591.

[26] S. M. Hatch, J. Briscoe, S. Dunn, *Adv. Mater.* **2013**, *25*, 867.

[27] E. Monroy, F. Omn s, F. Calle, *Semicond. Sci. Technol.* **2003**, *18*, R33.

[28] L. Sang, M. Liao, M. Sumiya, *Sensors* **2013**, *13*, 10482.

[29] L. Zheng, P. Yu, K. Hu, F. Teng, H. Chen, X. Fang, *ACS Appl. Mater. Interfaces* **2016**, *8*, 33924.

[30] L. Zhang, S. Bai, C. Su, Y. Zheng, Y. Qin, C. Xu, Z. L. Wang, *Adv. Funct. Mater.* **2015**, *25*, 5794.

[31] Y. Dong, Y. Zou, J. Song, Z. Zhu, J. Li, H. Zeng, *Nano Energy* **2016**, *30*, 173.

[32] Y.-Q. Bie, Z.-M. Liao, H.-Z. Zhang, G.-R. Li, Y. Ye, Y.-B. Zhou, J. Xu, Z.-X. Qin, L. Dai, D.-P. Yu, *Adv. Mater.* **2011**, *23*, 649.

[33] Y. Li, F. Della Valle, M. Simonnet, I. Yamada, J.-J. Delaunay, *Nanotechnology* **2009**, *20*, 45501.

[34] J. J. Hassan, M. A. Mahdi, S. J. Kasim, N. M. Ahmed, H. Abu Hassan, Z. Hassan, *Appl. Phys. Lett.* **2012**, *101*, 261108.

[35] Q. A. Xu, J. W. Zhang, K. R. Ju, X. D. Yang, X. Hou, *J. Cryst. Growth* **2006**, *289*, 44.

[36] W. Tian, T. Zhai, C. Zhang, S. L. Li, X. Wang, F. Liu, D. Liu, X. Cai, K. Tsukagoshi, D. Golberg, Y. Bando, *Adv. Mater.* **2013**, *25*, 4625.

[37] M. Grundmann, F. Klüpfel, R. Karsthof, P. Schlupp, F.-L. Schein, D. Splith, C. Yang, S. Bitter, H. von Wenckstern, *J. Phys. D: Appl. Phys.* **2016**, *49*, 213001.

[38] N. Park, K. Sun, Z. Sun, Y. Jing, D. Wang, *J. Mater. Chem. C* **2013**, *1*, 7333.

[39] M. Deo, S. Mujawar, O. Game, A. Yengantiwar, A. Banpurkar, S. Kulkarni, J. Jog, S. Ogale, *Nanoscale* **2011**, *3*, 4706.

[40] M. Ichimura, Y. Maeda, *Solid State Electron.* **2015**, *107*, 8.

[41] F. Teng, L. Zheng, K. Hu, H. Chen, Y. Li, Z. Zhang, X. Fang, *J. Mater. Chem. C* **2016**, *4*, 8416.

[42] B. D. Boruah, A. Mukherjee, A. Misra, *Nanotechnology* **2016**, *27*, 95205.

[43] Z. Y. Zhan, L. X. Zheng, Y. Z. Pan, G. Z. Sun, L. Li, *J. Mater. Chem.* **2012**, *22*, 2589.

[44] H. Chen, P. Yu, Z. Zhang, F. Teng, L. Zheng, K. Hu, X. Fang, *Small* **2016**, *12*, 5809.

[45] H. Ohta, M. Kamiya, T. Kamiya, M. Hirano, H. Hosono, *Thin Solid Films* **2003**, *445*, 317.

[46] R. Woods-Robinson, J. K. Cooper, X. Xu, L. T. Schelhas, V. L. Pool, A. Faghaninia, C. S. Lo, M. F. Toney, I. D. Sharp, J. W. Ager, *Adv. Electron. Mater.* **2016**, *2*, 1500396.

[47] X. Xu, J. Bullock, L. T. Schelhas, E. Z. Stutz, J. J. Fonseca, M. Hettick, V. L. Pool, K. F. Tai, M. F. Toney, X. Fang, A. Javey, L. H. Wong, J. W. Ager, *Nano Lett.* **2016**, *16*, 1925.

[48] W. Chamorro, T. S. Shyju, P. Boulet, S. Migot, P. Ghanbaja, P. Miska, P. Kuppusami, J. F. Pierson, *RSC Adv.* **2016**, *6*, 43480.

[49] H. P. Maruska, F. Namavar, N. M. Kalkhoran, *Appl. Phys. Lett.* **1992**, *61*, 1338.

[50] J. M. Shah, Y.-L. Li, T. Gessmann, E. F. Schubert, *J. Appl. Phys.* **2003**, *94*, 2627.

[51] X. A. Cao, E. B. Stokes, P. M. Sandvik, S. F. LeBoeuf, J. Kretchmer, D. Walker, *IEEE Electron Device Lett.* **2002**, *23*, 535.

[52] P. Schlupp, F.-L. Schein, H. von Wenckstern, M. Grundmann, *Adv. Electron. Mater.* **2015**, *1*, 1400023.

[53] A. M. Diamond, L. Corbellini, K. R. Balasubramaniam, S. Chen, S. Wang, T. S. Matthews, L.-W. Wang, R. Ramesh, J. W. Ager, *Phys. Status Solidi A* **2012**, *209*, 2101.

[54] M. G. Panthani, J. M. Kurley, R. W. Crisp, T. C. Dietz, T. Ezzyat, J. M. Luther, D. V. Talapin, *Nano Lett.* **2014**, *14*, 670.

[55] X. Chen, K. Ruan, G. Wu, D. Bao, *Appl. Phys. Lett.* **2008**, *93*, 112112.

[56] M. Cavas, R. K. Gupta, A. A. Al-Ghamdi, Z. Serbetci, Z. H. Gafer, F. El-Tantawy, F. Yakuphanoglu, *J. Electroceram.* **2013**, *31*, 260.

[57] C.-C. Wu, C.-F. Yang, *ACS Appl. Mater. Interfaces* **2013**, *5*, 4996.

[58] D.-Y. Wang, Y.-T. Jiang, C.-C. Lin, S.-S. Li, Y.-T. Wang, C.-C. Chen, C.-W. Chen, *Adv. Mater.* **2012**, *24*, 3415.

[59] Z. Yang, M. Wang, S. Shukla, Y. Zhu, J. Deng, H. Ge, X. Wang, Q. Xiong, *Sci. Rep.* **2015**, *5*, 11377.

[60] A. N. Banerjee, S. Nandy, C. K. Ghosh, K. K. Chattopadhyay, *Thin Solid Films* **2007**, *515*, 7324.

[61] Y. Xie, L. Wei, Q. Li, G. Wei, D. Wang, Y. Chen, J. Jiao, S. Yan, G. Liu, L. Mei, *Appl. Phys. Lett.* **2013**, *103*, 1.

[62] L. Zheng, F. Teng, Z. Zhang, B. Zhao, X. Fang, *J. Mater. Chem. C* **2016**, *4*, 33.